Water Vapor Budget in a Developing Tropical Cyclone and Its Implication for Tropical Cyclone Formation

CODY FRITZ AND ZHUO WANG

Department of Atmospheric Sciences, University of Illinois at Urbana–Champaign, Urbana, Illinois

(Manuscript received 25 November 2013, in final form 30 June 2014)

ABSTRACT

Evolution of the water vapor budget from the tropical wave stage to the tropical cyclone stage is examined using a high-resolution numerical model simulation. The focus is on a time window from 27 h prior to genesis to 9 h after genesis, and the diagnoses are carried out in the framework of the marsupial paradigm. Analysis shows that the vertically integrated inward moisture flux accounts for a majority of the total condensation and that its fractional contribution increases from the tropical wave stage to the tropical cyclone stage. The fractional contribution of the local evaporation is much smaller and decreases from the tropical wave stage to the tropical cyclone stage. It is also shown that the radial moisture flux above 850 hPa is rather weak prior to genesis but increases significantly after genesis because of the deepening of the inflow layer. The decrease in the fractional contribution of the local evaporation, or the increase in the fractional contribution of the vertically integrated inward moisture flux, is due to the strengthening of the low-level convergence associated with the secondary circulation. The intensification of the secondary circulation can be attributed to the organized convection and concentrated diabatic heating near the circulation center. The results suggest that the local evaporation and its positive interaction with the primary circulation may not be as important as generally appreciated for tropical cyclone development. By contrast, the increase in the fractional contribution by the inward moisture flux with the storm intensification implies the importance of the positive feedback among the primary circulation, the secondary circulation, and convection for tropical cyclone development.

1. Introduction

Moist convection is the primary driving force for tropical cyclone formation and intensification (Montgomery and Farrell 1993; Hendricks et al. 2004; Montgomery et al. 2006; Zhang and Sippel 2009; Wang 2012). The ultimate energy source of tropical cyclones comes from the warm ocean via the surface enthalpy flux. The release of latent heat concentrated near the circulation center drives the secondary circulation, increases the low-level moisture convergence, and intensifies the primary circulation.

There are several theories for tropical cyclone intensification. Charney and Eliassen (1964) and Ooyama (1964) proposed the conditional instability of the second kind (CISK) theory for the positive feedback between deep convection and the tropical cyclone vortex, and Ooyama (1982) proposed a cooperative theory. Although both theories emphasize the positive feedback between moist convection and the tropical cyclone vortex, Ooyama's theory differs from the CISK theory in that the CISK theory assumes the latent heat release of deep convection is proportional to the vertically integrated inward moisture flux and largely overlooks the role of the local evaporation, while the cooperative theory recognizes explicitly the importance of the surface moisture flux in maintaining convective instability and the intensification process. Emanuel (1987) proposed the wind-induced surface heat exchange (WISHE) mechanism, which emphasizes the positive feedback between the primary circulation and the surface heat fluxes. The recent study by Montgomery and Smith (2014), however, showed that a tropical cyclone could intensify without such a positive feedback in idealized numerical model simulations. They proposed an asymmetric pathway and suggested that tropical cyclones can intensify via rotating cumulonimbus clouds that grow in a vorticity-rich environment and amplify the local vorticity (Montgomery and Smith 2014).

It is an open question whether a unified theory exists for tropical cyclone formation and tropical cyclone

Corresponding author address: Cody Fritz, Department of Atmospheric Sciences, University of Illinois at Urbana–Champaign, 105 South Gregory St., Urbana, IL 61801.
E-mail: fritz7@illinois.edu

DOI: 10.1175/JAS-D-13-0378.1

intensification. Tropical cyclone formation is the process involving the formation and intensification of an incipient vortex. With much weaker surface wind speed and weaker and less organized deep convection, genesis may be different from the intensification of a tropical cyclone and is likely more susceptible to the environmental impacts. The WISHE theory highlights the finite-amplitude instability nature of tropical cyclogenesis. That is, the storm needs to exceed a certain intensity threshold to be amplified by a positive feedback. For this reason, Molinari et al. (2004) proposed that tropical cyclone formation consists of two stages: the pre-WISHE stage and the WISHE stage. Local surface enthalpy flux and its positive feedback with the primary circulation presumably intensify from the pre-WISHE stage to the WISHE stage. On the other hand, the system-scale moisture convergence is also expected to increase with the storm intensification. The relative importance of the local evaporation versus inward moisture flux at the pregenesis stage and the evolution of their relative contributions from the tropical wave stage to the tropical cyclone stage are not clear. Since the interaction among the primary circulation, the secondary circulation, and moist convection is the central issue of the controversy, a good understanding of the water vapor budget will help to better understand tropical cyclone formation and intensification. More specifically, if the system-scale moisture convergence becomes dominant with intensification, then the cooperative theory may be more relevant for tropical cyclone formation; if the contribution by the local evaporation becomes increasingly important, then the WISHE theory may be more relevant.

The water vapor budget for mature tropical cyclones has been examined in many previous studies using numerical model simulations or radar observations (Kurihara 1975; Marks and Houze 1987; Gamache et al. 1993; Zhang et al. 2002; Braun 2006; Yang et al. 2011). In a tropical cyclone simulation using an axisymmetric model, Kurihara (1975) showed that the overall moisture budget at the mature stage was dominated by the horizontal and vertical advection of water vapor and net condensation. Braun (2006) confirmed this result through the analysis of a high-resolution simulation of Hurricane Bonnie (1998). In particular, he showed that the ocean source of water vapor, specifically within the eyewall region, is quite small relative to the total net condensation and inward transport of water vapor. Yang et al. (2011) computed both the water vapor and condensate budgets using a high-resolution numerical model simulation of Typhoon Nari (2001) and showed that the net horizontal water vapor convergence for the whole storm accounted for 88% of the total net condensation within a 150-km radius.

The water vapor budget at the pregenesis stage, on the other hand, has not been well studied. Fritz and Wang (2013) showed that the mean vertical moisture transport plays the dominant role in moistening the free atmosphere in an incipient tropical cyclone and suggested that the upper troposphere is a potential weak spot for dry-air intrusion at the early stage of tropical cyclone development. Fritz and Wang (2013) also examined the radial and vertical distribution of the water vapor budget terms, the impacts of upper-level dry-air intrusion, and the difference between a developing wave and a nondeveloping wave.

In this study we will further examine the water vapor budget. In particular, we will examine the relative importance of the local evaporation versus inward moisture flux from the tropical wave stage to the tropical cyclone stage within the framework of the marsupial paradigm (Dunkerton et al. 2009). The marsupial paradigm hypothesizes that the cat's eye circulation within the critical layer of a tropical wave provides a favorable local environment for vorticity aggregation and convective organization that leads to tropical cyclone formation (Wang et al. 2010a,b; Wang 2012). It provides a quasi-Lagrangian framework to study the pregenesis evolution of the precursor disturbance. The numerical model and analysis methods are described in section 2. Results are presented and discussed in section 3, followed by a summary in section 4.

2. Model simulation and analysis description

a. *Numerical model simulation description*

The model used in this study is the Advanced Research Weather Research and Forecasting (ARW-WRF) Model, version 3.2.1 (Skamarock et al. 2005). The model is fully compressible and nonhydrostatic. A high-resolution numerical model simulation was conducted for Tropical Storm Fay (2008) by adopting a four-grid nested domain with horizontal grid spacing of 27, 9, 3, and 1 km. The outer two grids are fixed, while the inner two grids move with the pouch center (Wang 2014a,b; Fritz and Wang 2013). Convection was resolved explicitly at the grid scale except on the outermost mesh (27-km resolution), where the Kain–Fritcsh cumulus scheme (Kain 2004) was used. Other physics options include the Yonsei University planetary boundary layer scheme (Hong et al. 2006), the Dudhia (1989) shortwave radiation scheme, the Rapid Radiative Transfer Model (RRTM) longwave radiation scheme (Mlawer et al. 1997), and the WRF single-moment 6-class (WSM6) microphysics scheme. Prognostic water substance variables in the WSM6 scheme

include mixing ratios of water vapor, cloud water, cloud ice, snow, rain, and graupel (Hong and Lim 2006). Initial and boundary conditions were obtained from the Interim European Centre for Medium-Range Weather Forecasts (ECMWF) Re-Analysis (ERA-Interim) 6-hourly data.

Tropical Storm Fay (2008) developed from an African easterly wave (Brown et al. 2010). The wave propagated westward along a nearly zonal path and intensified into a tropical cyclone near Puerto Rico on 15 August. The synoptic-scale overview of the pre-Fay disturbance and the impacts of a transient dry-air intrusion on the storm development were examined in Fritz and Wang (2013). In addition, the statistics of convective processes and vertical vorticity from the tropical wave to the tropical cyclone stage and the cloud evolution and convective organization were examined by Wang (2014a,b) using the same model simulation. Readers are referred to Fritz and Wang (2013) and Wang (2014a,b) for more details regarding the storm evolution.

The simulation was started at 0000 UTC 13 August 2008 and ran 84 h until 1200 UTC 16 August 2008. A tropical depression forms at 0600 UTC 15 August in the model simulation, when a closed circulation develops at the surface (not shown), and a tropical storm forms at 1200 UTC 15 August, when the 10-m maximum wind speed exceeds 17 m s^{-1}. Both formation times in the model simulation are 6 h earlier than those in the National Hurricane Center (NHC) best-track data, and the errors between the best-track storm locations and the simulated pouch center locations at the corresponding times are less than 1° [see Fig. 1 in Wang (2014a)]. The favorable comparison of the simulated storm track and intensity with the NHC best-track data suggests that the model simulation captures the pregenesis evolution reasonably well.

The simulation covers the tropical wave, the tropical depression, and the tropical storm stages. This study will focus on the time frame between 0300 UTC 14 August and 1500 UTC 15 August. The diagnoses in the following section are carried out with respect to the wave pouch center at 1.5 km (~850 hPa), which was determined as the intersection of the critical latitude and the wave trough axis. The propagation speed of the precursor disturbance was estimated based on the Hovmöller diagram of total precipitable water and 700-hPa meridional winds (not shown). The average of the two speeds (−7.0 m s^{-1}) was used to determine the critical latitude.

b. Water vapor budget formulation

The water vapor budget equation in cylindrical coordinates can be written as

$$\frac{\partial q_v}{\partial t} = -\frac{1}{r}\frac{\partial (r q_v u)}{\partial r} - \frac{1}{r}\frac{\partial (q_v v)}{\partial \lambda} - \frac{\partial q_v w}{\partial z} + q_v\left[\frac{1}{r}\frac{\partial (ru)}{\partial r} + \frac{1}{r}\frac{\partial v}{\partial \lambda} + \frac{\partial w}{\partial z}\right] - \mathrm{NC} + B_v + R, \quad (1)$$

where q_v is the water vapor mixing ratio, r is the radius with respect to the pouch center, and u and w are the radial and vertical velocities in the wave comoving frame of reference, respectively. The term on the left-hand side (LHS) of the equation is the water vapor tendency in the wave comoving frame of reference; the first two terms on the right-hand side (RHS) are the horizontal moisture flux convergence and the vertical moisture flux convergence, respectively. The third term is the divergence term, NC represents the net condensation (positive values mean condensation and deposition exceeding evaporation and sublimation) per unit mass, B_v represents the contribution of the planetary boundary layer processes to the vapor budget per units mass, and R is the residual term. NC and B_v are output directly from the model, and the remaining terms are derived from the WRF Model output.

To evaluate the water vapor budget for a layer between two pressure surfaces, we can integrate Eq. (1). Using the continuity equation and the divergence theorem, we have

$$\int_\tau \frac{\partial \rho q_v}{\partial t} d\tau = -\frac{r_0}{g}\int_{P_2}^{P_1}\int_0^{2\pi} q_v u \, d\lambda \, dp + \int_0^{r_0}\int_0^{2\pi} r\rho q_v w \, d\lambda \, dr\Big|_{P_2}^{P_1} - \int_\tau \rho \mathrm{NC} \, d\tau + \int_\tau \rho B_v \, d\tau, \quad (2)$$

where τ represents the volume [$d\tau = dxdydz = -r/(\rho g) d\lambda dr dp$], ρ is the density of dry air, g represents gravitational constant, P_1 and P_2 are the bottom and top pressure surfaces, respectively, r_0 is the radius of the cylinder, and λ is the azimuth. The term on the LHS is the volume-integrated water vapor tendency (TEN), the first term on the RHS is the inward moisture flux (HFX) between P_1 and P_2, the second term is the difference of the vertical moisture flux (VFX) between the top and bottom pressure surfaces (or the net vertical moisture influx), and the last two terms are the volume-integrated net condensation (NC) and the oceanic source term (OS) related to the planetary boundary layer processes, respectively. The 3D divergence term in Eq. (1) is negligible (i.e., the flow is approximately incompressible) and has been dropped from Eq. (2) (Braun 2006; Fritz and Wang 2013). The residual term includes diffusion and artificial source terms by setting negative mixing ratios to zero and is small compared to

HFX, VFX, and NC. We will exclude the residual term in our following analysis for simplicity, which does not affect our conclusion on the relative importance of the OS and HFX terms.

For the planetary boundary layer, since the vertical velocity and the vertical moisture flux at the surface are nearly zero, the budget equation can be simplified to

$$\mathrm{TEN} = \mathrm{HFX} - \mathrm{VFX}(850) - \mathrm{NC} + \mathrm{OS}, \qquad (3)$$

where VFX(850) is the upward moisture flux at the top of the planetary boundary layer (the negative sign indicates the moisture flux out of the layer).

Above the boundary layer, OS can be neglected. The budget equation is reduced to

$$\mathrm{TEN} = \mathrm{HFX} + [\mathrm{VFX}(P_1) - \mathrm{VFX}(P_2)] - \mathrm{NC}, \qquad (4)$$

where VFX(P_1) and VFX(P_2) are the upward moisture flux across the bottom and top pressure surfaces, respectively. The budget terms are evaluated within 200 km of the pouch center in the following section. The robustness of the results with respect to the radius is examined in section 3.

c. Description of tropospheric layers

The water vapor budget is examined for three tropospheric layers: the planetary boundary layer (PBL), the lower-troposphere layer (LTL), and the upper-troposphere layer (UTL). The PBL is where strong horizontal moisture convergence occurs and is the water vapor reservoir for convection and condensation in the free troposphere (Gamache et al. 1993; Braun 2006; Fritz and Wang 2013). Intensification of the primary circulation is closely related to the boundary layer convergence (e.g., Wang 2012). Budget analysis within the PBL helps to understand the roles of the positive feedback between the surface wind and the local evaporation (i.e., the WISHE mechanism; Emanuel 1986, 1987; Neelin et al. 1987; Rotunno and Emanuel 1987) and the positive feedback between the primary circulation and the secondary circulation in tropical cyclone formation. We define the PBL as a layer below 850 hPa, although the top of the boundary layer can extend above 850 hPa for a tropical cyclone. The LTL is defined as the layer between 850 and 500 hPa, and the UTL is defined as the layer between 500 and 100 hPa. Moistening of the lower to middle troposphere has been suggested to be important for genesis (Wang 2012; Nolan 2007; Braun 2010). Wang (2014b) showed that cumulus congestus plays a dominant role in moistening the lower to middle troposphere prior to genesis and that moistening of the upper troposphere is mainly due to deep convection. Since 500 hPa is close to the mean height of congestus clouds, it is used to separate the upper and lower troposphere.

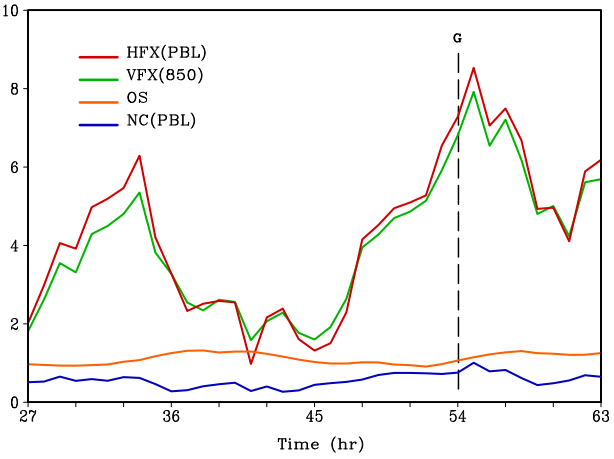

FIG. 1. Horizontal moisture flux (red curve), vertical moisture flux (green curve), net condensation (blue curve), and ocean source (orange curve) in the PBL within a 200-km radius of the pouch center from 0300 UTC 14 Aug (27 h) to 1500 UTC 15 Aug (63 h). The units are $10^7\,\mathrm{kg\,s^{-1}}$. Time of genesis in the model simulation (i.e., 54 h) is denoted by "G."

3. Water vapor budget analysis

a. Planetary boundary layer

For the water vapor budget in the PBL, we will address three specific questions: (i) What is the major water vapor balance in the PBL? (ii) What is the relative contribution of the local evaporation within the wave pouch compared to the horizontal moisture convergence from outside of the pouch? (iii) Does the fractional contribution of the local evaporation increase as the disturbance transitions from a tropical wave to a tropical cyclone?

To address the first question, the time series of HFX (PBL), VFX(850), NC(PBL), and OS are shown in Fig. 1 for a 200-km radius from the pouch center. VFX(PBL) and HFX(PBL) have similar magnitudes and vary in phase. Both are much larger than NC(PBL) and OS. This suggests that the primary moisture source within the PBL is the inward moisture flux and the primary moisture sink is the upward moisture transport; or, in other words, the local evaporation makes a small contribution to the moisture supply. While HFX(PBL) and VFX(850) are both subject to the modulation of the diurnal cycle and peak around 1000 UTC, there is a discernible increasing trend as the storm intensifies.

To evaluate the relative contribution by the local evaporation, we calculate the ratio of the ocean source term to the horizontal moisture flux across a 200-km radius below 850 hPa (Fig. 2) from 0300 UTC 14 August

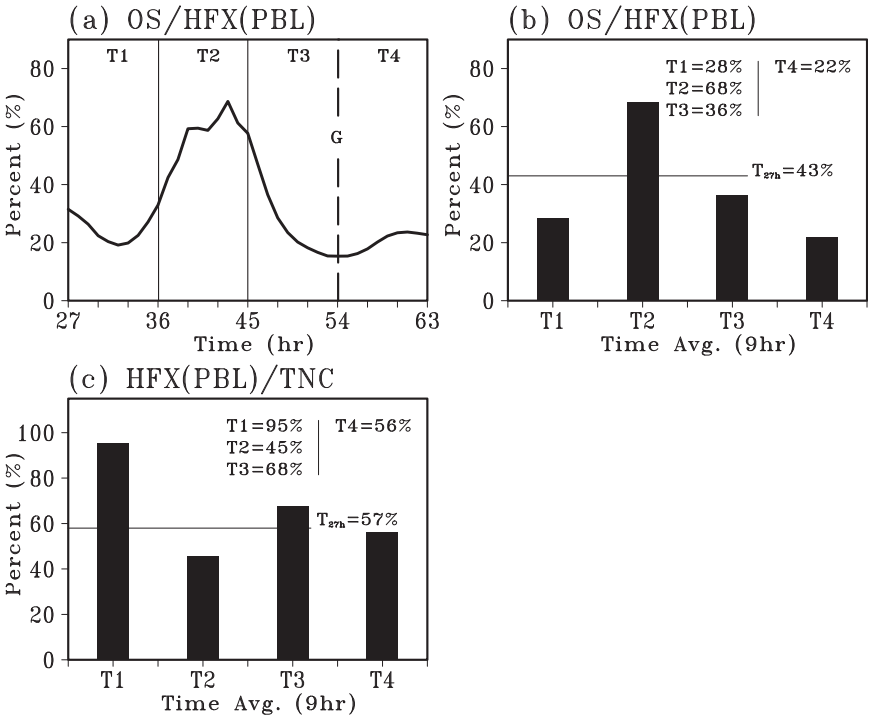

FIG. 2. (a) The ratio of the ocean source of water vapor to the horizontal moisture flux within a 200-km radius in the PBL (solid curve), (b) the ratios of the ocean source to the inward moisture flux during different time periods, and (c) the ratios of the horizontal moisture flux to the total net condensation during different time periods. The vertical dashed line denotes the genesis time in (a). In (b) and (c) T1–T4 represent 9-h increments beginning at 0300 UTC 14 Aug and ending at 1500 UTC 15 Aug, and the black horizontal line represents the 27-h average prior to genesis T_{27h}.

to 1500 UTC 15 August 2008. The ocean source term represents the contribution by the local evaporation within the wave pouch. The ratio varies from 20% during peak convective periods (i.e., 0300–1200 UTC) to about 70% in nonpeak convective periods, and the large variability is mainly due to the diurnal variation of HFX. The ratio averaged over a few 9-h periods before (T1, T2, and T3) and after genesis (T4) is shown in Fig. 2b. Prior to genesis, the ratio is approximately 28%–36% during the peak convective periods (T1 and T3) and approximately 68% during the nonpeak convective period (T2), with an average of 43% for the 27-h time period. Following genesis, the local evaporation accounts for about 22% of the inward moisture transport within the PBL. The number is close to Yang et al.'s (2011) finding that the evaporation from the ocean's surface accounts for 11% of the inward horizontal vapor transport within the boundary layer of Typhoon Nari (2001). The quantitative difference in the ratios between our study and Yang et al. (2011) is likely related to different storm intensities. Although the budget terms are subject to the impacts of the diurnal cycle, the reduced ratio of OS to HFX(PBL) after genesis cannot simply be attributed to the diurnal cycle because the postgenesis mean ratio is lower than the mean ratio during any of the three pregenesis periods. It suggests that the horizontal moisture convergence makes a major and increasing contribution to the moisture supply. The decreasing relative contribution by the local evaporation (or the increasing relative contribution by the horizontal moisture convergence) with the storm intensification suggests that the positive feedback between the primary circulation and the secondary circulation, rather than the positive feedback between wind speed and the local evaporation, plays an important role in tropical cyclone development.

Since the boundary layer is the moisture reservoir, it is illuminating to examine the contribution of the boundary layer moisture convergence to the total net condensation within an air column. Figure 2c shows the ratio of the PBL horizontal moisture influx to the total net condensation between 1000 and 100 hPa for the same 9-h periods as in Fig. 2b. The ratio varies between 45% and 95% prior to genesis, where the maximum ratio coincides with the time of peak convection. Interestingly, the ratio of the boundary layer HFX to the total NC at the tropical cyclone stage (56%) is lower than the mean ratio prior to genesis (68%). As shown later in this section, the decrease in this ratio is due to the deepening of the

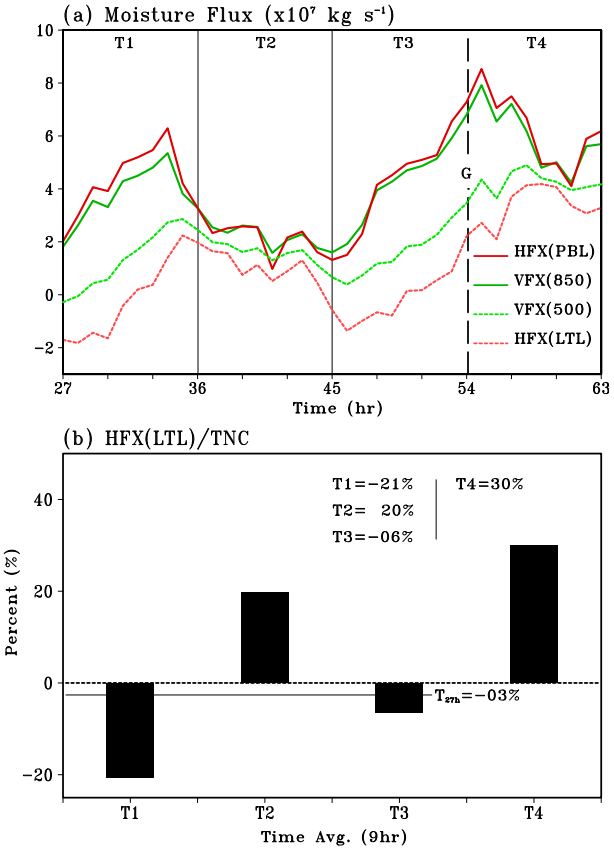

FIG. 3. (a) Time series of the horizontal moisture flux in the PBL (red solid curve) and in the LTL (red dashed curve), and the vertical moisture flux at 850 (green solid curve) and 500 hPa (green dashed curve); (b) the ratios of the horizontal flux in the LTL to the total net condensation within a 200-km radius. The gray solid line in (b) represents the pregenesis average over 27 h.

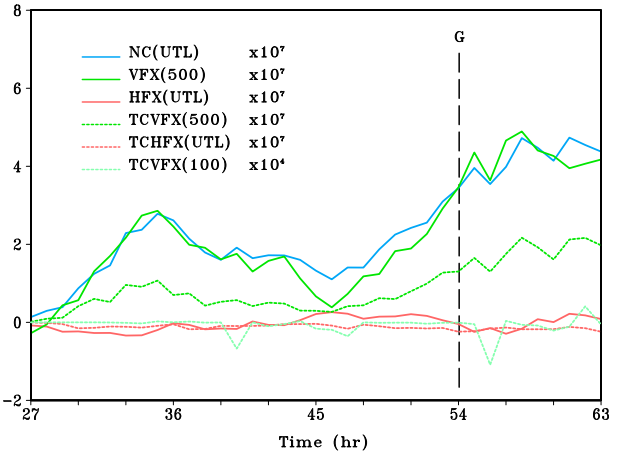

FIG. 4. Major vapor budget terms (kg s^{-1}) in the upper-tropospheric layer: net condensation [NC(UTL); blue solid curve], vertical moisture flux at 500 hPa [VFX(500); green solid curve], horizontal moisture flux [HFX(UTL); red solid curve], vertical moisture flux of total condensate [TCVFX(500); green dashed curve], horizontal moisture flux of total condensate [TCHFX(UTL); red dashed curve], and vertical moisture flux of total condensate across 100 hPa [TCVFX(100); light green dashed curve].

secondary circulation and the increasing inward moisture transport in the lower troposphere.

b. *Middle and upper troposphere*

The time series of the horizontal moisture influx in the lower to midtroposphere is shown in Fig. 3a. Prior to genesis, HFX within the LTL (Fig. 3a) has strong fluctuations between positive and negative values and is much weaker than HFX in the PBL at most times. Horizontal moisture convergence in the LTL increases approaching genesis and becomes comparable to that in the PBL, which is owing to a deeper inflow layer at the tropical cyclone stage than at the tropical wave stage. To better illustrate this increase, Fig. 3b shows the ratio of the net horizontal moisture flux in the LTL to the total condensation in the column between 1000 and 100 hPa. Following genesis, the horizontal moisture transport above the PBL accounts for 30% of the total condensation in comparison to −3% (27-h average) prior to genesis.

Also shown in Fig. 3a are the vertical moisture fluxes through 850 hPa (from the PBL to the LTL) and through 500 hPa (from the LTL to UTL). VFX(850) and VFX (500) both have a strong diurnal cycle, and the former exceeds the latter by up to 60%. Also, note that VFX (500) and HFX(500) have similar magnitudes and vary in phase but slightly lag behind VFX(850) and HFX (PBL), and the amplification of the HFX, both in the PBL and LTL, coincides with peak convection (see the time series of the total NC in Fig. 6a).

The major vapor balance in the upper troposphere persists between NC and the upward moisture transport across 500 hPa [VFX(500)] (Fig. 4). This suggests that deep convection transports moisture into the upper troposphere (>500 hPa) and that water vapor is removed from the column via condensation or deposition. The horizontal moisture flux is below but close to zero, indicating weak outward water vapor transport in the upper troposphere. The vertical moisture flux across 100 hPa (not shown) is also much smaller than NC(UTL) or VFX (500). NC(UTL) and VFX(500) vary in phase and peak around 35 h (1100 UTC), which is consistent with the diurnal cycle of deep convection. An increasing trend is discernible in both time series. As a reference, the horizontal and vertical fluxes of total condensate (cloud water, ice, snow, and graupel) are also shown in Fig. 4. It is shown that the vertical flux of total condensate across 500 hPa [TCVFX(500)] is much larger than the horizontal flux of total condensate [TCHFX(UTL)]. Also, the vertical flux of total condensate across 100 hPa [TCVFX

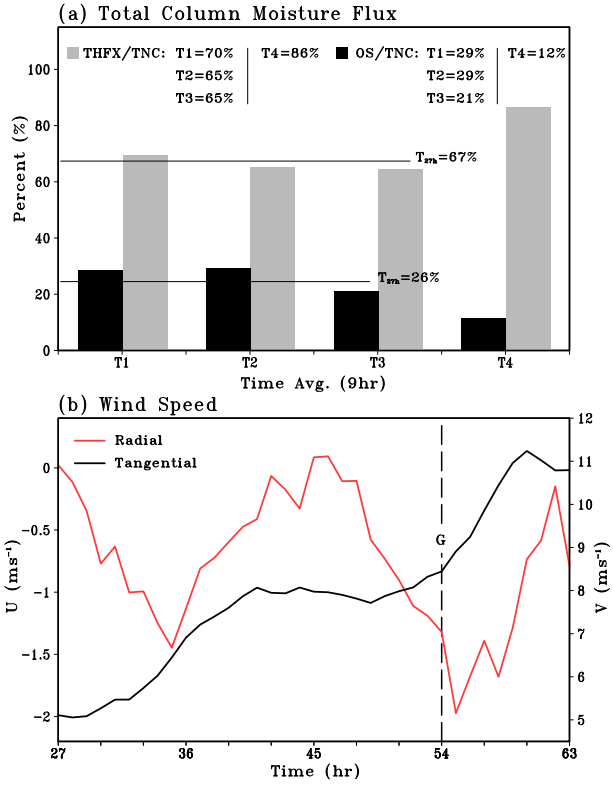

FIG. 5. (a) Ratios of the horizontal flux (gray) and the ocean source (black) to the total net condensation in four 9-h periods and (b) radial (red curve) and tangential (black curve) wind speeds at a 200-km radius from 9-km domain. The two horizontal lines in (a) indicate the pregenesis averages over 27 h (T1–T3).

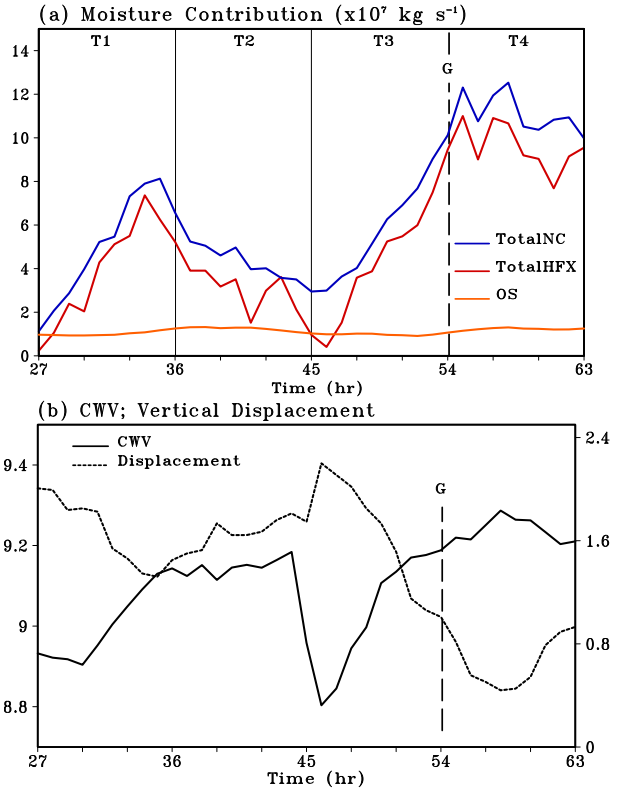

FIG. 6. (a) Time series of the total NC (blue solid curve), total HFX (red solid curve), and ocean source (orange solid curve), and (b) time series of the column water vapor (solid curve; 10^{12} kg) and horizontal distance between the 1.5- and the 5-km pouch center (dashed curve; °).

(100)], or the transport of hydrometeor due to overshooting, is also quite small.

c. *Water vapor budget for the tropospheric column*

Figure 5 shows the contributions by the vertically integrated inward moisture flux and the ocean source term to the total net condensation in the column within a 200-km radius at different time periods. Despite the strong diurnal cycle of convection prior to genesis, the ratio of the vertically integrated inward moisture flux to the total net condensation is rather steady and is close to two-thirds. After genesis, the ratio increases to 86%. The contribution of OS is much smaller and is between about 20% and 30% prior to genesis, dropping to 12% after genesis.[1] The decrease in the fractional contribution of the local evaporation, or the increase in the fractional contribution of the total horizontal moisture influx, is due to the strengthening of the low-level convergence associated with the secondary circulation (see the time series of the 900-hPa azimuthally averaged radial flow in Fig. 5b). The intensification of the secondary circulation can be attributed to the organized convection and the concentrated diabatic heating near the center of the circulation (see Fig. 7 and the discussion in section 3d). On the other hand, the organized and intense convection is fueled by the strong low-level moisture convergence, and the significant intensification of the tropical cyclone vortex follows the peak convection and occurs with the strong low-level convergence (see radial and tangential wind speeds in Fig. 5b and the total net condensation in Fig. 6a). The system-scale intensification due to the low-level convergence has been examined in some previous studies (e.g., Tory and Montgomery 2008; Wang et al. 2010a; Montgomery and Smith 2010; Fang and Zhang 2010; Raymond et al. 2011). Briefly speaking, the increasing fractional contribution of the horizontal moisture convergence with the storm intensity reflects the positive feedback among the

[1] The sum of the two ratios, THFX/TNC and OS/TNC, is not 100% owing to the variation of the column water vapor or the nonzero tendency term (TEN) (Fig. 6).

TABLE 1. Ratios at different radii (i.e., 100 and 300 km) for OS and HFX within the PBL, HFX within the PBL and total NC, HFX in the lower troposphere and total NC, and total HFX and total NC.

Time average (h)	OS/HFX(PBL)		HFX(PBL)/total NC	
	100 km	300 km	100 km	300 km
27–36	0.18	0.27	1.43	1.06
36–45	0.42	1.22	0.86	0.40
45–54	0.38	0.17	0.94	0.48
27–54	0.26	0.50	1.11	0.66
54–63	0.09	0.33	0.65	0.53
	HFX(LTL)/total NC		Total HFX/total NC	
	100 km	300 km	100 km	300 km
27–36	−0.55	0.02	0.84	0.99
36–45	−0.10	0.22	0.83	0.63
45–54	−0.30	0.05	0.74	0.57
27–54	−0.32	0.09	0.82	0.74
54–63	0.28	0.24	0.90	0.78

primary circulation, the secondary circulation, and convection.

d. Results for different radii

Analyses of the moisture budget at other radii were investigated to test the robustness of the results. Table 1 compares the 100- and 300-km radii, respectively. Despite the quantitative differences, the calculations with the 100- and 300-km radii support the findings with a 200-km radius: (i) the local evaporation makes a much smaller contribution to the total moisture supply than the inward moisture transport on average, and the ratio of the local evaporation to HFX(PBL) decreases from the tropical wave stage to the tropical cyclone stage; (ii) the contribution of the vertically integrated inward moisture flux (i.e., the total HFX) to the vertically integrated net condensation (total NC) increases from the tropical wave stage to the tropical cyclone stage, which implies that the contribution by the local evaporation decreases; and (iii) the inward moisture transport in the boundary layer makes a major contribution (>50%) to the total condensation, and the inward moisture flux in the lower troposphere increases significantly after genesis. On the other hand, Table 1 also shows that the fractional contribution by the local evaporation increases with increasing radius (or area). For example, the local evaporation accounts for 50% of the inward moisture transport in the boundary layer moisture within a 300-km radius during the 27-h pregenesis time period and exceeds the inward moisture transport during 36–45 h, a time period of inactive convection. It is also worth noting that the horizontal moisture transport in the lower troposphere (850–500 hPa) is rather weak at different radii prior to genesis (varying from −32% to 9% of the total NC on average).

Table 1 also shows that the ratio of the total HFX to the total NC has large fluctuations and is rather low during T3, a time period of reduced convection (indicated by the drop in total net condensation in Fig. 6a). The drop of the ratio is due to a substantial reduction of the total inward moisture flux around 45 h instead of a significant increase in the OS term. The decrease in the total inward moisture flux is accompanied by a decrease in the column water vapor (CWV) at 45 h and coincides with a large vertical displacement between the low-level vortex core and the upper-level vortex core (Fig. 6b). In comparison, variations of CWV are inversely related to the vertical displacement of the pouch center between 1.5- and 5-km altitudes. This is consistent with Raymond and Lopez Carrillo's (2011) and Wang et al.'s (2012) findings that a vertically aligned wave pouch provides a deep protected region from environmental influences.

Figure 7 shows the vertical profiles of horizontal moisture flux, vertical flux, and net condensation averaged with different radii (100, 200, and 300 km) over 24 h leading up to and following genesis. All the variables increase after genesis. It is worth noting that the areal averages increase with decreasing radius. The stronger inward moisture flux and stronger vertical moisture flux in the inner pouch region indicate organized convection near the pouch center. The concentrated diabatic heating (Fig. 7c) effectively drives the transverse circulation, increases the low-level moisture convergence, and intensifies the primary circulation via vortex stretching. Figure 7a also provides the visualization for the deepening inflow layer after genesis, especially for a 100-km radius.

e. Model sensitivity experiment

To test the sensitivity of the finding to the model physics, a series of sensitivity experiments were carried out. We first completed a simulation with the same model physics and configuration as the control run, except that the innermost grid with the resolution of 1 km was dropped. The evolution of the storm and water vapor budget terms from this simulation (''Coarse'') is close to that from the control run (Fig. 8), suggesting that the water vapor budget is not very sensitive to the model resolution. To save computational time, we thus adopted the configuration of three nested grids (with resolutions of 27, 9, and 3 km) for the sensitivity experiments (Table 2).

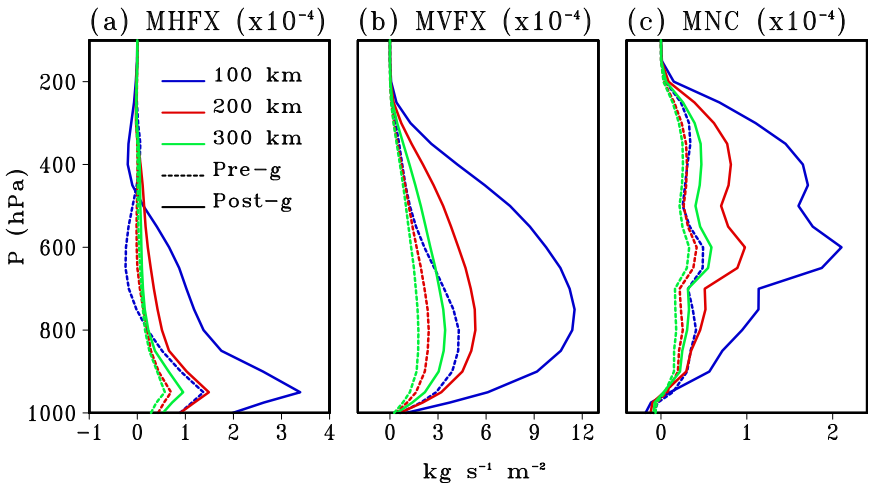

FIG. 7. (a) Azimuthal-mean horizontal moisture flux (positive for inward flux), (b) areal-mean vertical flux, and (c) areal-mean net condensation for radii of 100 (blue curve), 200 (red curve), and 300 km (green curve). Dashed curves represent a temporal average of 24 h prior to genesis and solid curves represent a temporal average of 24 h after genesis.

Goddard (Tao et al. 1989) and Lin (Lin et al. 1983) schemes were used to test the sensitivity to the microphysics schemes. Sensitivity to the surface bulk drag and enthalpy coefficients was also analyzed. The WRF-ARW Model has three options for the air–sea flux parameterizations: options 0, 1, and 2. These options differ in the exchange coefficients for drag C_D, sensible heat C_H, and latent heat C_Q (Green and Zhang 2013). In option 0, C_D is equal to C_H and larger than C_Q. The three exchange coefficients all increase monotonically with wind speed. In option 1, C_D, C_H, and C_Q all level off at high wind speeds. Option 2 has the same C_D as option 1, but C_H and C_Q are smaller than those in option 1 and decrease slightly with wind speed at high wind speeds. Among the three options, option 0 has the largest C_H and C_Q except at very weak wind speeds ($<\sim 3\,\mathrm{m\,s^{-1}}$). Readers are referred to Green and Zhang (2013) for more technical details. Although options 1 and 2 were suggested to be more realistic than option 0, the simulations with WSM6 and option 1 or 2 and the simulation using Lin and option 2 did not produce a tropical cyclone. This could be due to error compensation in the model, and it is also possible that the air–sea flux parameterization in option 0 does not perform too badly for a weak tropical cyclone like Fay. We also tested different boundary layer schemes: the Mellor–Yamada–Janjic (Eta) TKE scheme, the Mellor–Yamada–Nakanishi–Niino (MYNN) third-level TKE scheme, and the medium-range forecast (MRF) scheme. Unfortunately, none of these simulations produced a tropical cyclone. The five simulations that produce a tropical cyclone were examined and compared to the control run. Although the simulation using WSM6 and option 1 did not produce a tropical cyclone, it was also examined for reference.

Figure 8a shows the 10-m wind speed evolution from 0300 UTC 14 August to 1500 UTC 15 August 2008 for the sensitivity experiments as well as the control run. Not surprisingly, there exists noticeable variability in the storm intensification. However, all experiments except WSM6Opt1 produce a tropical cyclone by time $t = 63$ h. Figure 8b shows the ratio of the ocean source term to the horizontal moisture flux across a 200-km radius below 850 hPa (the same as the calculations in Fig. 2). Despite the large spread, the local evaporation term is smaller than the horizontal moisture convergence term, and the ratio of the local evaporation to HFX decreases after genesis in all sensitivity experiments when compared to the 27-h pregenesis average (see Table 2). In most experiments, the 9-h postgenesis average is smaller than any of the three 9-h pregenesis averages. These results are consistent with our findings using the high-resolution control run.

4. Conclusions and discussion

The evolution of the water vapor budget of Tropical Storm Fay (2008) from the tropical wave stage to the tropical cyclone stage was examined using a high-resolution numerical model simulation. We focused on a time window from 27 h prior to genesis to 9 h after genesis, and the diagnoses were carried out in the framework of the marsupial paradigm. It was found that the primary moisture source within the PBL is the

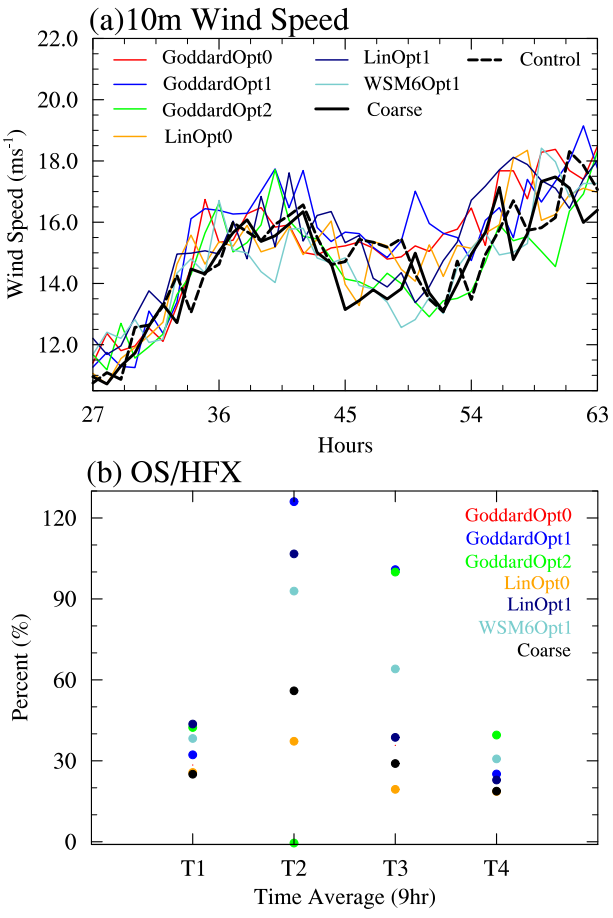

FIG. 8. (a) Time series of the 10-m wind speed and (b) the ratio of the ocean source of water vapor to the total inward moisture flux within a 200-km radius for different sensitivity experiments: GoddardOpt0 (red), GoddardOpt1 (blue), GoddardOpt2 (green), LinOpt0 (orange), LinOpt1 (navy blue), WSM6Opt1 (gray), and Coarse (black). T1–T4 in (b) represent 9-h increments beginning at 0300 UTC 14 Aug and ending at 1500 UTC 15 Aug.

inward moisture flux and the primary moisture sink is the upward moisture transport. The local evaporation makes a smaller contribution than the inward moisture flux, and its fractional contribution decreases from the tropical wave stage to the tropical cyclone stage. The horizontal moisture transport between 850 and 500 hPa is much weaker than that in the boundary layer prior to genesis, but it increases significantly after genesis because of the deepening of the inflow. It is also shown that vertical moisture transport plays the dominant role in moistening the free atmosphere, as suggested by Fritz and Wang (2013). For the upper troposphere, the major vapor balance persists between the net condensation–deposition and the upward moisture transport across 500 hPa.

Conclusions drawn from the vapor budget of Fay (2008) solicit some questions about the importance of the local evaporation in tropical cyclone development. Previous studies emphasized the positive feedback between the ocean surface heat fluxes and the primary circulation for tropical cyclone intensification (Emanuel 1986, 1987; Rotunno and Emanuel 1987). The WISHE theory assumes a symmetric balanced model. A stronger negative radial gradient of specific humidity or equivalent potential temperature leads to a stronger warm-core structure and an increase in tangential wind speed under the thermal wind balance. While this description succinctly describes the control of the boundary layer thermodynamics on the storm intensification and suggests that a stronger surface wind speed would likely induce stronger surface heat flux (with which we agree), our diagnosis implies that the increase in specific humidity or equivalent potential temperature near the circulation center and thus a stronger radial gradient are primarily contributed by the inward moisture flux. This suggests that the role of the local evaporation and its positive interaction with the primary circulation may not be as important as generally appreciated. By contrast, the increase in the fractional contribution by the inward moisture flux (in the PBL and the lower troposphere) with the storm intensification implies the importance of the positive feedback between the primary circulation and the secondary circulation for tropical cyclone development.

This study, however, should not be interpreted as saying that the local evaporation is not important for tropical cyclone formation. As shown in Fig. 2, the local evaporation is 60%–70% of the horizontal moisture influx in the PBL in the inactive phase of convection. It

TABLE 2. Sensitivity experiments completed with changes in the microphysics schemes and surface bulk drag and enthalpy coefficients and the ratio of the ocean source to the horizontal moisture flux in the PBL within a 200-km radius.

Experiment	Microphysics	PBL	Air–sea flux	TC	OS/HFX_{PBL} T_{27h} (%)	OS/HFX_{PBL} T4 (%)
Coarse	WSM6	YSU	0	Y	36	19
WSM6Opt1	—	—	1	N	63	31
GoddardOpt0	Goddard	—	0	Y	40	22
GoddardOpt1	Goddard	—	1	Y	70	25
GoddardOpt2	Goddard	—	2	Y	53	40
LinOpt0	Lin	—	0	Y	27	19
LinOpt1	Lin	—	1	Y	62	23

suggests that the local evaporation plays an important, but not dominant, role in replenishing the column moisture when convection is inactive and the low-level convergence is relatively weak.

To simplify the budget evaluation in different layers, we set the boundary layer height as a constant. This way we can exclude the contribution of a varying boundary layer height to the variations of the HFX(PBL). One could argue that the boundary layer depth increases in a more convectively active condition, and the fractional contribution of the HFX(PBL) would be even larger with an increasing boundary layer depth. Also note that the ratio of OS to the total HFX (or the total NC) is independent of the boundary layer depth. The assumption of a constant PBL height thus does not affect our results qualitatively. The robustness of the results is also confirmed by further sensitivity tests with different model physics. On the other hand, this study is admittedly based on the numerical model simulation of a single storm, and whether the findings can be generalized warrants further study. It would also be interesting to examine how the fractional contribution of the local evaporation to the total net condensation varies with the intensity change of a hurricane.

Acknowledgments. This research was supported by the National Science Foundation Grants AGS-1016095 and AGS-1118429. The authors thank three anonymous reviewers for the constructive comments. The ERA-Interim data were downloaded from the Research Data Archive at the National Center for Atmospheric Research, Computational and Information Systems Laboratory (NCAR CISL). Computational support for numerical model simulation and data storage was also provided by the NCAR CISL.

REFERENCES

Braun, S. A., 2006: High-resolution simulation of Hurricane Bonnie (1998). Part II: Water budget. *J. Atmos. Sci.,* **63,** 43–64, doi:10.1175/JAS3609.1.

——, 2010: Reevaluating the role of the Saharan air layer in Atlantic tropical cyclogenesis and evolution. *Mon. Wea. Rev.,* **138,** 2007–2037, doi:10.1175/2009MWR3135.1.

Brown, D. P., J. L. Beven, J. L. Franklin, and E. S. Blake, 2010: Atlantic hurricane season of 2008. *Mon. Wea. Rev.,* **138,** 1975–2001, doi:10.1175/2009MWR3174.1.

Charney, J. G., and A. Eliassen, 1964: On the growth of the hurricane depression. *J. Atmos. Sci.,* **21,** 68–75, doi:10.1175/1520-0469(1964)021<0068:OTGOTH>2.0.CO;2.

Dudhia, J., 1989: Numerical study of convection observed during the Winter Monsoon Experiment using a mesoscale two-dimensional model. *J. Atmos. Sci.,* **46,** 3077–3107, doi:10.1175/1520-0469(1989)046<3077:NSOCOD>2.0.CO;2.

Dunkerton, T. J., M. T. Montgomery, and Z. Wang, 2009: Tropical cyclogenesis in a tropical wave critical layer: Easterly waves. *Atmos. Chem. Phys.,* **9,** 5587–5646, doi:10.5194/acp-9-5587-2009.

Emanuel, K. A., 1986: An air–sea interaction theory for tropical cyclones. Part I: Steady-state maintenance. *J. Atmos. Sci.,* **43,** 585–604, doi:10.1175/1520-0469(1986)043<0585:AASITF>2.0.CO;2.

——, 1987: An air–sea interaction model of intraseasonal oscillations in the tropics. *J. Atmos. Sci.,* **44,** 2324–2340, doi:10.1175/1520-0469(1987)044<2324:AASIMO>2.0.CO;2.

Fang, J., and F. Zhang, 2010: Initial development and genesis of Hurricane Dolly (2008). *J. Atmos. Sci.,* **67,** 655–672, doi:10.1175/2009JAS3115.1.

Fritz, C., and Z. Wang, 2013: A numerical study of the impacts of dry air on tropical cyclone formation: A development case and a nondevelopment case. *J. Atmos. Sci.,* **70,** 91–111, doi:10.1175/JAS-D-12-018.1.

Gamache, J. F., R. A. Houze Jr., and F. D. Marks Jr., 1993: Dual-aircraft investigation of the inner core of Hurricane Norbert. Part III: Water budget. *J. Atmos. Sci.,* **50,** 3221–3243, doi:10.1175/1520-0469(1993)050<3221:DAIOTI>2.0.CO;2.

Green, B. W., and F. Zhang, 2013: Impacts of air–sea flux parameterizations on the intensity and structure of tropical cyclones. *Mon. Wea. Rev.,* **141,** 2308–2324, doi:10.1175/MWR-D-12-00274.1.

Hendricks, E. A., M. T. Montgomery, and C. A. Davis, 2004: The role of "vortical" hot towers in the formation of Tropical Cyclone Diana (1984). *J. Atmos. Sci.,* **61,** 1209–1232, doi:10.1175/1520-0469(2004)061<1209:TROVHT>2.0.CO;2.

Hong, S.-Y., and J. O. J. Lim, 2006: The WRF Single-Moment Microphysics Scheme (WSM6). *J. Korean Meteor. Soc.,* **42,** 129–151.

——, Y. Noh, and J. Dudhia, 2006: A new vertical diffusion package with an explicit treatment of entrainment processes. *Mon. Wea. Rev.,* **134,** 2318–2341, doi:10.1175/MWR3199.1.

Kain, J. S., 2004: The Kain–Fritsch convective parameterization: An update. *J. Appl. Meteor.,* **43,** 170–181, doi:10.1175/1520-0450(2004)043<0170:TKCPAU>2.0.CO;2.

Kurihara, Y., 1975: Budget analysis of a tropical cyclone simulated in an axisymmetric numerical model. *J. Atmos. Sci.,* **32,** 25–59, doi:10.1175/1520-0469(1975)032<0025:BAOATC>2.0.CO;2.

Lin, Y.-L., R. D. Farley, and H. D. Orville, 1983: Bulk parameterization of the snow field in a cloud model. *J. Climate Appl. Meteor.,* **22,** 1065–1092, doi:10.1175/1520-0450(1983)022<1065:BPOTSF>2.0.CO;2.

Marks, F. D., and R. A. Houze Jr., 1987: Inner-core structure of Hurricane Alicia from airborne Doppler radar observations. *J. Atmos. Sci.,* **44,** 1296–1317, doi:10.1175/1520-0469(1987)044<1296:ICSOHA>2.0.CO;2.

Mlawer, E. J., S. J. Taubman, P. D. Brown, M. J. Iacono, and S. A. Clough, 1997: Radiative transfer for inhomogeneous atmosphere: RRTM, a validated correlated-k model for the longwave. *J. Geophys. Res.,* **102** (D14), 16 663–16 682, doi:10.1029/97JD00237.

Molinari, J., D. Vollaro, and K. L. Corbosiero, 2004: Tropical cyclone formation in a sheared environment: A case study. *J. Atmos. Sci.,* **61,** 2493–2509, doi:10.1175/JAS3291.1.

Montgomery, M. T., and B. F. Farrell, 1993: Tropical cyclone formation. *J. Atmos. Sci.,* **50,** 285–310, doi:10.1175/1520-0469(1993)050<0285:TCF>2.0.CO;2.

——, and R. K. Smith, 2010: Tropical-cyclone formation: Theory and idealized modeling. *Proc. Seventh Int. Workshop on Tropical Cyclones,* La Réunion, France, WMO, 2.1. [Available online at http://www.meteo.physik.uni-muenchen.de/~roger/Publications/IWTC-VII_topic_2.1.pdf.]

——, and ——, 2014: Paradigms for tropical-cyclone intensification. *Aust. Meteor. Oceanogr. J.,* in press.

——, M. E. Nicholls, T. A. Cram, and A. B. Saunders, 2006: A vortical hot tower route to tropical cyclogenesis. *J. Atmos. Sci.,* **63,** 355–386, doi:10.1175/JAS3604.1.

Neelin, J. D., I. M. Held, and K. H. Cook, 1987: Evaporation-wind feedback and low-frequency variability in the tropical atmosphere. *J. Atmos. Sci.,* **44,** 2341–2348, doi:10.1175/1520-0469(1987)044<2341:EWFALF>2.0.CO;2.

Nolan, D. S., 2007: What is the trigger for tropical cyclogenesis? *Aust. Meteor. Mag.,* **56,** 241–266.

Ooyama, K., 1964: A dynamical model for the study of tropical cyclone development. *Geofis. Int.,* **4,** 187–198.

——, 1982: Conceptual evolution of the theory and modeling of the tropical cyclone. *J. Meteor. Soc. Japan,* **60,** 369–379.

Raymond, D. J., and C. Lopez Carrillo, 2011: The vorticity budget of developing Typhoon Nuri (2008). *Atmos. Chem. Phys.,* **11,** 147–163, doi:10.5194/acp-11-147-2011.

——, S. L. Sessions, and C. López Carrillo, 2011: Thermodynamics of tropical cyclogenesis in the northwest Pacific. *J. Geophys. Res.,* **116,** D18101, doi:10.1029/2011JD015624.

Rotunno, R., and K. Emanuel, 1987: An air–sea interaction theory for tropical cyclones. Part II: Evolutionary study using a non-hydrostatic axisymmetric numerical model. *J. Atmos. Sci.,* **44,** 542–561, doi:10.1175/1520-0469(1987)044<0542:AAITFT>2.0.CO;2.

Skamarock, W. C., J. B. Klemp, J. Dudhia, D. O. Gill, D. M. Barker, W. Wang, and J. G. Powers, 2005: A description of the advanced research WRF version 2. NCAR Tech. Note NCAR/TN-468+STR, 88 pp.

Tao, W.-K., J. Simpson, and M. McCumber, 1989: An ice-water saturation adjustment. *Mon. Wea. Rev.,* **117,** 231–235, doi:10.1175/1520-0493(1989)117<0231:AIWSA>2.0.CO;2.

Tory, K. J., and M. T. Montgomery, 2008: Tropical cyclone formation: A synopsis of the internal dynamics. *Extended Abstracts, 28th Conf. on Hurricanes and Tropical Meteorology,* Orlando, FL, Amer. Meteor. Soc., 10A.1. [Available online at http://ams.confex.com/ams/28Hurricanes/techprogram/paper_138062.htm.]

Wang, Z., 2012: Thermodynamic aspects of tropical cyclone formation. *J. Atmos. Sci.,* **69,** 2433–2451, doi:10.1175/JAS-D-11-0298.1.

——, 2014a: Characteristics of convective processes and vertical vorticity from the tropical wave to the tropical cyclone stage in the high-resolution numerical model simulations of Tropical Cyclone Fay (2008). *J. Atmos. Sci.,* **71,** 896–915, doi:10.1175/JAS-D-13-0256.1.

——, 2014b: Role of cumulus congestus in tropical cyclone formation in a high-resolution numerical model simulation. *J. Atmos. Sci.,* **71,** 1681–1700, doi:10.1175/JAS-D-13-0257.1.

——, M. T. Montgomery, and T. J. Dunkerton, 2010a: Genesis of pre–Hurricane Felix (2007). Part I: The role of the wave critical layer. *J. Atmos. Sci.,* **67,** 1711–1729, doi:10.1175/2009JAS3420.1.

——, ——, and ——, 2010b: Genesis of pre–Hurricane Felix (2007). Part II: Warm core formation, precipitation evolution, and predictability. *J. Atmos. Sci.,* **67,** 1730–1744, doi:10.1175/2010JAS3435.1.

——, ——, and C. Fritz, 2012: A first look at the structure of the wave pouch during the 2009 PREDICT–GRIP dry runs over the Atlantic. *Mon. Wea. Rev.,* **140,** 1144–1163, doi:10.1175/MWR-D-10-05063.1.

Yang, M.-J., S. A. Braun, and D.-S. Chen, 2011: Water budget of Typhoon Nari (2001). *Mon. Wea. Rev.,* **139,** 3809–3828, doi:10.1175/MWR-D-10-05090.1.

Zhang, D. L., Y. Liu, and M. K. Yau, 2002: A multi-scale numerical study of Hurricane Andrew (1992). Part V: Inner-core thermodynamics. *Mon. Wea. Rev.,* **130,** 2745–2763, doi:10.1175/1520-0493(2002)130<2745:AMNSOH>2.0.CO;2.

Zhang, F., and J. A. Sippel, 2009: Effects of moist convection on hurricane predictability. *J. Atmos. Sci.,* **66,** 1944–1961, doi:10.1175/2009JAS2824.1.